Amit Datye
Department of Materials Science and Engineering,
University of Tennessee,
Knoxville, TN 37996

Lin Li
Department of Materials Science and Engineering,
University of Tennessee,
Knoxville, TN 37996

Wei Zhang
Department of Materials Science and Engineering,
University of Tennessee,
Knoxville, TN 37996

Yujie Wei
LNM,
Institute of Mechanics,
Chinese Academy of Sciences,
Beijing 100190, China

Yanfei Gao[1]
Department of Materials Science and Engineering,
University of Tennessee,
Knoxville, TN 37996;
Materials Science and Technology Division,
Oak Ridge National Laboratory,
Oak Ridge, TN 37831
e-mail: ygao7@utk.edu

George M. Pharr[1]
Department of Materials Science and Engineering,
University of Tennessee,
Knoxville, TN 37996;
Materials Science and Technology Division,
Oak Ridge National Laboratory,
Oak Ridge, TN 37831
e-mail: pharr@utk.edu

Extraction of Anisotropic Mechanical Properties From Nanoindentation of SiC-6H Single Crystals

Because brittle solids fail catastrophically during normal tension and compression testing, nanoindentation is often a useful alternative technique for measuring their mechanical properties and assessing their deformation characteristics. One practical question to be addressed in such studies is the relationship between the anisotropy in the uniaxial mechanical behavior to that in the indentation response. To this end, a systematic study of the mechanical behavior the 6H polytype of a hexagonal silicon carbide single crystal (SiC-6H) was performed using standard nanoindentation methods. The indentation elastic modulus and hardness measured using a Berkovich indenter at a peak load of 500 mN varied over a wide range of crystal orientation by only a few percent. The variation in modulus is shown to be consistent with an anisotropic elastic contact analysis based on the known single crystal elastic constants of the material. The variation in hardness is examined using a single crystal plasticity model that considers the anisotropy of slip in hexagonal crystals. When compared to experimental measurements, the analysis confirms that plasticity in SiC-6H is dominated by basal slip. An anisotropic elastic contact analysis provides insights into the relationship between the pop-in load, which characterizes the transition from elasticity to plasticity during nanoindentation testing, and the theoretical strength of the material. The observations and analyses lay the foundations for further examination of the deformation and failure mechanisms in anisotropic materials by nanoindentation techniques. [DOI: 10.1115/1.4033790]

Keywords: nanoindentation, elastic and plastic anisotropy, basal slip

1 Introduction

Silicon carbide (SiC) has many attractive, application-specific mechanical properties such as high Young's modulus (~450 GPa), high hardness, good flexural strength, good high-temperature creep resistance, low density, and good wear resistance. These are all attributable to the material's intrinsic strong covalent bonding. Because SiC is also less costly compared to other high-hardness materials, it has become a popular material for a variety of automotive, aerospace, and high-temperature applications, as well as for use in microelectromechanical systems [1–3].

Among SiC's numerous single crystalline forms, which have similar thermomechanical but different electrical and optical properties, here we focus the behavior of the common 6H polytype. The method used for the investigation is nanoindentation, which has a distinct advantage over conventional tensile or compression testing in that the hydrostatic constraint imposed by the indenter inhibits fracture and thereby allow for studies of plastic deformation rather than just catastrophic brittle behavior. For brittle solids, indentation tests are often used to measure various mechanical properties related to plasticity, such as hardness, which are often anisotropic due to anisotropies in slip. For example, Shaffer [4] studied the hardness anisotropy in SiC-6H single crystals using a Knoop indenter with a 100-gram load by indenting on the $(10\bar{1}0)$ and $(11\bar{2}0)$ planes with the long axis of the Knoop indenter lying parallel or perpendicular to the $\langle 0001 \rangle$ direction. The maximum Knoop hardness was found to be 29.17 GPa when indenting in the $\langle 0001 \rangle$ direction with the long axis parallel to $\langle 11\bar{2}0 \rangle$ direction, and the minimum value was 21.29 GPa when indenting in the $\langle 10\bar{1}0 \rangle$ direction with the long axis parallel to the $\langle 0001 \rangle$ direction. However, such hardness measurements alone cannot determine many important details of the deformation behavior.

It is generally accepted that only a few slip systems can be activated in SiC-6H due to its hexagonal structure and that dislocation motion experiences a much higher lattice resistance for some slip systems than the others. Indentation tests have been combined

[1]Corresponding authors.

Contributed by the Applied Mechanics Division of ASME for publication in the Journal of Applied Mechanics. Manuscript received May 2, 2016; final manuscript received May 29, 2016; published online June 22, 2016. Editor: Yonggang Huang.

with microscopy observations and surface slip trace analysis to determine the slip systems in some cases [5–8]. In SiC-6H, it has been shown that the dominant slip system on which plastic deformation occurs is $(0001)\langle 11\bar{2}0\rangle$ at low temperatures and $(10\bar{1}0)\langle 11\bar{2}0\rangle$ at high temperatures. Moreover, Page et al. [8] found that when indenting in $\langle 0001\rangle$ direction with a Berkovich indenter, plasticity is controlled entirely by basal dislocations that form in a highly symmetric rosette geometry that is consistent with a stress analysis based on an anisotropic elastic contact analysis in similar materials, i.e., hexagonally close packed (HCP) Ti and Mg single crystals [9,10]. Microscopy analysis of slip traces is quite cumbersome to conduct, and conventional hardness tests using Knoop, Brinell, or Vickers indenters do not provide load–displacement information even though indentation load–displacement data often contain important clues about the deformation processes and can be used to separate the relative importance of elastic and plastic deformation. Such information is routinely obtained in nanoindentation tests, which are capable of obtaining indentation load–displacement data with nanometer displacement and micronewton load resolution [11,12]. However, an important question that arises in analyzing such data is: How is it influenced by material anisotropy, both elastic and plastic?

To address this and other related questions, nanoindentation experiments were conducted on SiC-6H single crystals in various crystallographic orientations. Materials and experimental details are given in Sec. 2. The dependence of the effective indentation modulus on the crystallographic orientation is compared with a theoretical contact analysis in Sec. 3. In Sec. 4, the measured hardness anisotropy is analyzed by a crystal plasticity model with good agreement between simulation and experiment obtained, but only when slip is chosen to be the basal $\langle a\rangle$ system. Section 5 investigates indentation pop-in, which represents the transition from elastic to plastic deformation caused by the homogeneous nucleation of dislocations at the theoretical strength and allows one to estimate the theoretical strength on the active slip system. The findings are summarized in Sec. 6.

2 Materials and Nanoindentation Experiments

Single crystalline 6H-SiC samples were obtained from Cree Research, Inc. (Durham, NC; denoted here as Cree SiC-6H) and also from Nitride Crystals, Inc. (Deer Park, NY; denoted here as NC SiC-6H). The Cree SiC-6H crystals were provided as wafers about 250 μm in thickness with the normal to the wafer surface in the [1] direction (c-axis wafers), and the NC SiC-6H material as cubes about 1 cm size. For tests in a second crystallographic direction, a piece of the semiconductor-grade Cree SiC-6H wafer was fractured along a cleavage plane perpendicular to the wafer surface to produce a surface for indentation in the $\langle a\rangle$ direction. This was mounted in resin, ground with a series of SiC abrasive papers, and polished with Buehler MasterMet 2 noncrystallizing colloidal silica (SiO_2) polishing suspension (0.02 μm) using a vibratory polishing machine.

The crystal orientations used in the indentation experiments were defined relative to the zenith angle θ shown in Fig. 1(*a*). Two indentation orientations were examined for Cree the SiC-6H samples, $\theta = 0$ deg or $\langle 0001\rangle$ (the wafer surface), and $\theta = 90$ deg or $\langle 1\bar{2}10\rangle$, the cleavage plane perpendicular to the $\langle a\rangle$ axis. The NC SiC-6H crystals were cut with a diamond saw in several different orientations to provide normals falling in plane 1 in Fig. 1(*a*). These samples were mounted in resin and mechanically ground with several grades SiC, followed by a 120-hr colloidal silica polish using the vibratory polisher. The orientations of the polished NC SiC-6H samples were determined using Laue back reflection X-ray techniques in conjunction with the software package ORIENTEXPRESS to determine the exact zenith angle, θ. A total of four crystallographic orientations ($\theta = 0$, 35, 44, and 90 deg) were used in the nanoindentation tests. For the inclined angles, the maximum misalignment was within ± 2.5 deg of the target value. To examine possible orientation deviations from the plane

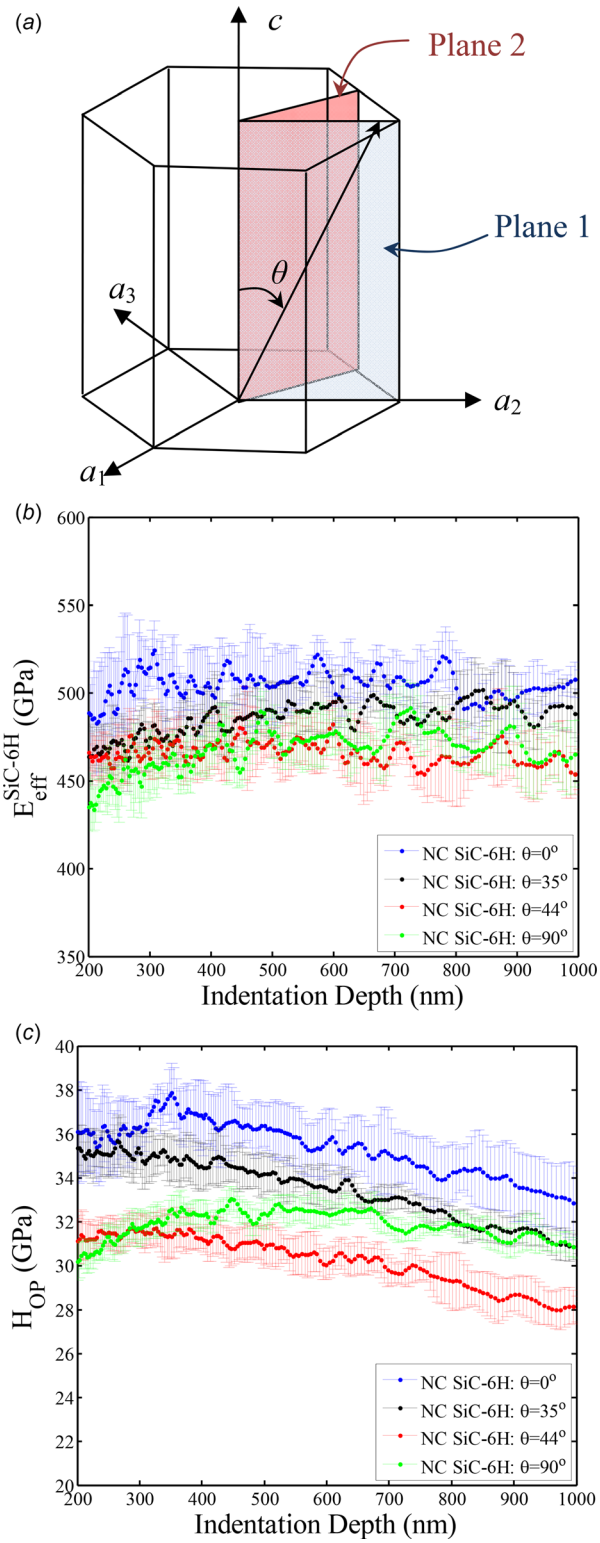

Fig. 1 (*a*) Schematic diagram showing the zenith angle defined in the lattice prism relative to the indentation direction. In the experiments, the zenith angle was varied in plane 1. Plane 2 is also defined to indicate maximum possible deviation of the indentation direction from the plane 1. ((*b*) and (*c*)) Depth dependence of the indentation modulus and hardness obtained using the Oliver–Pharr method for NC SiC-6H single crystals with four zenith angles.

defining the zenith angle, we also consider a second plane (plane 2) shown in Fig. 1(*a*) that is spanned by $\langle 0001 \rangle$ and $\langle \bar{1}100 \rangle$.

The nanoindentation tests were performed using a Nanoindenter XP system (MTS Nano Instruments, Oak Ridge, TN) with Berkovich and spherical diamond indenters up to a maximum peak load of 500 mN. To obtain the indentation modulus and hardness as a function of indentation depth, the continuous stiffness measurement (CSM) technique was employed [11]. Scanning electron microscopy (SEM) with a Zeiss Auriga dual beam FIB/SEM instrument was used to image some of the residual impressions for measurement of contact areas in a manner that accounts for pile-up. Since standard nanoindentation measurements do not account for pile-up effects, the imaging was done to obtain a more accurate measure of the true contact area, which is needed in the calculation of hardness and modulus from the nanoindentation load–displacement data [11]. A Nikon interference microscope was also used to characterize the height of the pile-up for some of the indentations. The Cree SiC-6H samples were indented using both the Berkovich indenter and several spherical indenters with different radii, with the latter used to study pop-in phenomenon. In contrast, only Berkovich indentations were used for the NC SiC-6H samples.

3 Anisotropy in Indentation Modulus

Effects of elastic anisotropy on nanoindentation measurements have been documented in an analysis by Vlassak and Nix [13,14]. For a pair of solids in frictionless contact, the contact stiffness, or the stiffness during unloading for elastic–plastic contact, is given by

$$S = \frac{dP}{dh} = 2E_r\sqrt{\frac{A}{\pi}} \tag{1}$$

where the reduced modulus E_r combines the effective indentation moduli of the indenter and specimen through the relation $E_r = [(1/E_{\text{eff}}^{\text{indenter}}) + (1/E_{\text{eff}}^{\text{specimen}})]^{-1}$. The relationship in Eq. (1) is one of the fundamental equations used in the Oliver–Pharr analysis method of nanoindentation data [11]. For elastically isotropic materials with Young's modulus, E_{specimen}, and Poisson's ratio, ν_{specimen}, the effective specimen modulus is given by $E_{\text{eff}}^{\text{specimen}} = E_{\text{specimen}}/(1-\nu_{\text{specimen}}^2)$, but the relation is much more complex for elastically anisotropic solids and must be evaluated in other ways as discussed elsewhere [13–16]. For purposes of the analysis here, the diamond indenter is assumed to be elastically isotropic with Young's modulus $E_{\text{indenter}} = 1141$ GPa and Poisson's ratio $\nu_{\text{indenter}} = 0.07$, for which the corresponding effective modulus of the indenter is $E_{\text{eff}}^{\text{indenter}} = E_{\text{indenter}}/(1-\nu_{\text{indenter}}^2) = 1147$ GPa.

Experimentally, the Oliver–Pharr method determines the indentation moduli from the measurement of the contact stiffness and the contact area in Eq. (1). Basic nanoindentation measurements of $E_{\text{eff}}^{\text{SiC-6H}}$ obtained using the CSM technique are shown in Fig. 1(*b*) for NC SiC-6H in various crystal orientations. The modulus so determined shows no dependence on the indentation depth, confirming that the machine stiffness and area function used to evaluate the data are adequate. The average values of modulus and their standard variations obtained from at least 20 tests are given in Table 1 for the Cree SiC-6H and in Table 2 for the NC SiC-6H samples, where the subscript OP refers to the Oliver–Pharr method. As mentioned previously, one drawback of the Oliver–Pharr analysis procedure is that it does not properly account for the effects of pile-up on the contact area, which can have important influences on both the measured modulus and hardness [17]. In this study, SEM and optical profilometry confirmed that there is indeed measurable pile-up around the indentations. We correct for it here by directly measuring the actual contact areas in SEM images, A_{actual}, and using them in the Oliver–Pharr analysis to determine the effective modulus from Eq. (1) and the hardness from $H = P/A_{\text{actual}}$. Corrected values computed in this way are included in Tables 1 and 2, designated with the subscript corrected. The effective elastic moduli of the SiC-6H computed in each of these ways are plotted as a function of zenith angle in Fig. 2(*a*). The indentation modulus can also be calculated from a theoretical analysis of anisotropic elastic contact [13–16]. Results are given by the solid curve in Fig. 2(*a*) using the following elastic constants: $C_{11} = 501$ GPa, $C_{12} = 111$ GPa, $C_{13} = 52$ GPa, $C_{33} = 553$ GPa, and $C_{44} = 163$ GPa. Note that the shape of the theoretical curve generally matches well with the experimental data.

From Fig. 2(*a*), we observe a difference of about 7% between the highest (at $\theta = 0$ deg) and the lowest (at $\theta = 44$ deg) values $E_{\text{eff}}^{\text{SiC-6H}}$, indicating a small but measurable anisotropy in the indentation modulus. There is also a difference between the two SiC-6H materials, possibly due to the type and level of dopants incorporated in the crystals. However, it should be noted that the elastic constants used in the analytical calculation, as obtained from Brillouin scattering experiment, have an uncertainty that may be as high as 10%. Thus, within experimental uncertainty, all the measured values agree reasonably well with the theoretically calculated $E_{\text{eff}}^{\text{SiC-6H}}$ provided the pile-up correction is applied. Without correcting for pile-up, the effective elastic moduli are too high. Similar pile-up effects on hardness and modulus measurement have been documented in experiments and finite element simulations [17].

4 Determining Slip Anisotropy From Indentation Hardness Anisotropy

The indentation depth dependence of the Oliver–Pharr hardness, H_{OP}, is shown in Fig. 1(*c*). The hardness decreases slowly with depth, indicating an indentation size effect, as is observed in many materials [18]. Values of H_{OP} averaged over the depth range 150–900 nm are given in Table 1 for the Cree material and in Table 2 for the NC single crystals. The tables also include the corrected hardness values, $H_{\text{corrected}}$, determined using the actual contact areas from images obtained in the SEM at a peak indentation load of 500 mN. The corrected hardnesses are smaller than H_{OP} because of the pile-up effects.

Figure 2(*b*) presents the hardnesses plotted as a function of zenith angle, θ. For the Cree SiC-6H single crystals, only the *c*-axis and *a*-axis orientations were measured, with the differences in hardness being less than a few percent. The dependence of H on θ is thus better illustrated from the measurements on the NC SiC-6H single crystals. This material exhibits a minimum in hardness at $\theta = 44$ deg, but as with the modulus, the degree of hardness anisotropy is not particularly large. These results are consistent with the Knoop indentation tests of Shaffer [4], who observed a hardness of 30 GPa in the $\langle 0001 \rangle$ direction and about 25 GPa and 26 GPa when indenting on the $\{10\bar{1}0\}$ and $\{1\bar{2}10\}$ planes, respectively.

Table 1 Indentation modulus and hardness and corresponding values corrected for pile-up for Cree SiC-6H single crystals in two orientations measured by nanoindentation with a Berkovich indenter

Zenith angle in Cree SiC-6H (deg)	$E_{\text{eff}}^{\text{SiC-6H}}\|_{\text{OP}}$ (GPa)	$E_{\text{eff}}^{\text{SiC-6H}}\|_{\text{corrected}}$ (GPa)	H_{OP} (GPa)	$H_{\text{corrected}}$ (GPa)
0	549.7 ± 20.6	503.1 ± 28.2	41.0 ± 1.2	32.3 ± 1.5
90	513.7 ± 19.8	461.9 ± 22.5	39.1 ± 0.8	30.8 ± 2.1

Table 2 Indentation modulus and hardness and corresponding values corrected for pile-up for NC SiC-6H single crystals in four different orientations measured by nanoindentation with a Berkovich indenter

Zenith angle in NC SiC-6H (deg)	$E_{\text{eff}}^{\text{SiC-6H}}\|_{\text{OP}}$ (GPa)	$E_{\text{eff}}^{\text{SiC-6H}}\|_{\text{corrected}}$ (GPa)	H_{OP} (GPa)	$H_{\text{corrected}}$ (GPa)
0	497.2 ± 9.4	460.2 ± 8.4	36.8 ± 1.0	31.6 ± 0.7
35	471.9 ± 5.7	444.3 ± 8.7	35.3 ± 0.8	30.3 ± 1.1
44	461.2 ± 6.0	439.0 ± 7.2	31.6 ± 0.6	27.1 ± 0.5
90	468.3 ± 3.8	448.8 ± 6.1	32.1 ± 0.4	27.5 ± 0.7

Even though the degree of hardness anisotropy in Fig. 2(*b*) is small, the hardness data are sufficient to explore the underlying slip anisotropy by comparison to the predictions of a crystal plasticity model. For a single crystal that deforms by dislocation slip obeying Schmid's law, the crystal plasticity framework is well established [19–25]. The total deformation gradient, $\mathbf{F}$, can be decomposed in the plastic part, $\mathbf{F}^p$, due to dislocation slip, and the elastic part, $\mathbf{F}^e$, that considers elastic stretching and rigid body rotation. The rate of the plastic part of the deformation gradient, $\dot{\mathbf{F}}^p$, relates to the slip rates on all the slip systems through the kinematic relationship

$$\dot{\mathbf{F}}^p\mathbf{F}^{p-1} = \sum_{\alpha} \dot{\gamma}^{(\alpha)}\mathbf{s}^{(\alpha)} \otimes \mathbf{m}^{(\alpha)} \tag{2}$$

where "−1" denotes the inverse of the tensor, $\dot{\gamma}^{(\alpha)}$ is the slip rate on the α-th slip system, $\mathbf{s}^{(\alpha)}$ and $\mathbf{m}^{(\alpha)}$ are unit vectors of the slip direction and the slip plane normal, and $\otimes$ denotes the tensor product. When the resolved shear stress on a given slip system reaches the critical resolved shear stress (CRSS), the plastic deformation takes place and a set of hardening relationships have to be specified. Here, our objective is to determine which slip system governs the resulting hardness anisotropy, so that the hardening behavior is not considered. The elastic constants are well known (given in Sec. 3), so that the only adjustable parameters are the CRSSs on the slip systems.

The above crystal plasticity model has been implemented by Staroselsky and Anand for hexagonal crystals as a user-defined material subroutine (VUMAT) in the commercial finite element software package, ABAQUS [19,20]. Note that in our indentation tests, while we know the indentation direction, the crystallographic directions along the three faces of the Berkovich indenter were not controlled or measured. Thus, a finite element model has been constructed using a conical indenter with a half-apex angle of 70.3 deg to represent the Berkovich indenter. The specimen was meshed into $39 \times 39 \times 11$ rectangular elements of the C3D8R type in ABAQUS. The contact size was much smaller than the specimen dimensions, so the bottom and side surfaces of the specimen were prescribed with fixed boundary conditions. The hardness value was obtained by linear fitting of the $P \sim h^2$ curve. As will be explained later, the indentation effective strain is significantly large so that the contact response falls into the plastic regime. In our crystal plasticity finite element simulations, we assumed that only one type of slip system operates and ignored the hardening behavior, so that the only adjustable parameter is the CRSS of the chosen slip system.

In Fig. 3, the dependence of the simulated hardness on the zenith angle is illustrated for four different common HCP slip systems: (1) basal slip, (2) prismatic slip, (3) pyramidal slip in the $\langle a \rangle$ direction, and (4) pyramidal slip in the $\langle a+c \rangle$ direction. As a first observation, we note that the measured hardness in Fig. 3(*a*) agrees nearly perfectly with the crystal plasticity simulation for basal slip provided we choose a CRSS of $\tau_{\text{CRSS}} = 4.8$ GPa from curve fitting. When using the same CRSS value but choosing different slip systems, we find that the relationships between hardness and zenith angle in Figs. 3(*b*)–3(*d*) are very different and do not match well with the trends in the experimental data. Note that we are mostly interested here in the trends in the data rather than the values since the values could be changed by choosing different CRSSs. Prior experiments such as the TEM study by Page et al. [8] have suggested the dominant slip system at room temperature is indeed the basal $\langle a \rangle$ slip system. The agreement in Fig. 3(*a*) suggests that this slip system is indeed responsible for the variation, albeit small, in the indentation hardness. Second, it should be noted that the stress fields under the indentation contact are much more complicated than those in uniaxial tests. For a uniaxial test of a hexagonal crystal indented in the *c*-axis or *a*-axis directions, the Schmid factor on the basal slip system vanishes, so no plastic deformation can be observed. The Schmid factor for the uniaxial test reaches a maximum at an intermediate zenith angle in a manner that varies with the square of the zenith angle, that is, a

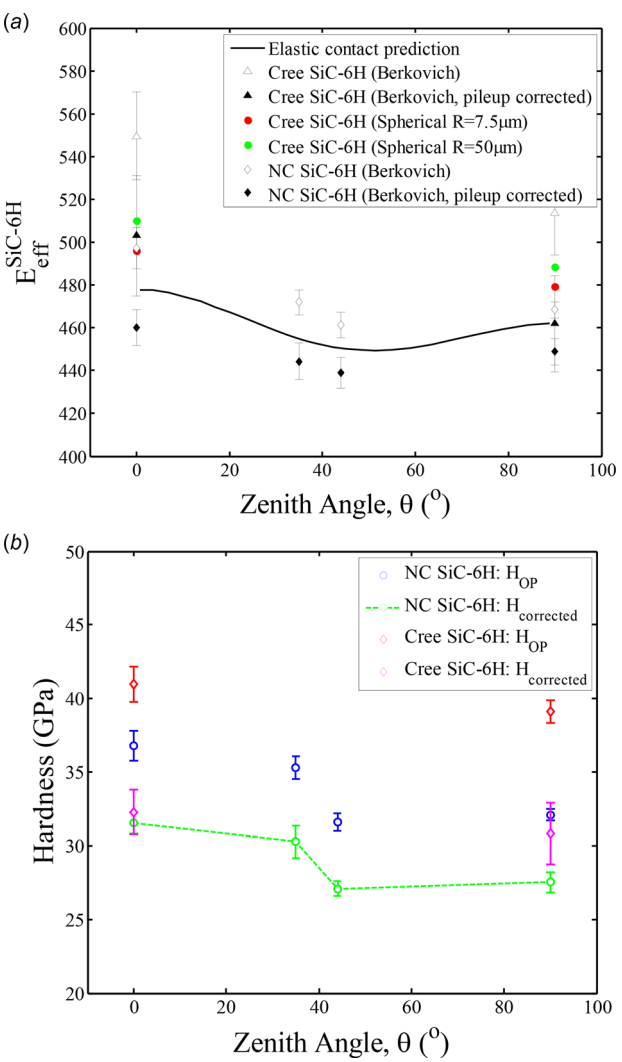

Fig. 2 (*a*) Effective indentation modulus and (*b*) hardness for both Cree and NC SiC-6H single crystals plotted as a function of zenith angle. The measured effective indentation moduli agree well with those predicted from anisotropic elastic contact analysis.

parabolic dependence. On the other hand, for the indentation-induced stress fields, indenting in the c-axis and a-axis directions produces a large resolved shear stress on the basal slip system. This will be discussed further in Sec. 5 as it is related to the "indentation Schmid factor."

The trends in the data in Fig. 3(*a*) also appear to resemble the dependence of the effective elastic modulus $E_{\text{eff}}^{\text{SiC}-6\text{H}}$ on the zenith angle in Fig. 2(*a*). Presumably, this resemblance is merely coincidental since the indentation is not just elastic but elastic–plastic for the following reasons. The ratio of hardness to τ_{CRSS} is about 7 from Fig. 3(*a*). For the plastic contact response, the constraint factor, i.e., the ratio of hardness to uniaxial yield stress, σ_Y, is about 2.8. We may relate σ_Y to τ_{CRSS} by $\sqrt{3}$ through the relationship between Mises shear stress to pure shear, or by the Taylor factor of 3 that relates single crystal to polycrystal yield strengths. Both will agree with the finding of $H/\tau_{\text{CRSS}} \approx 7$ in Fig. 3(*a*). In addition, the effective strain measure for the 70.3 deg conical indenter [26,27], $E_{\text{eff}}\text{ctg}70.3\,\text{deg}/H$, suggests that the indentation response is in the elastic–plastic stage.

Indentation tests on cubic crystals do not usually show such a variation in hardness with respect to the indentation direction because of the large number of slip systems in FCC and BCC lattices. Results similar to Fig. 3 have been reported in a number of recent studies of HCP Mg single crystals [22–25]. However, while the slip behavior in Mg obeys the same kinematic relationship of Eq. (2), twinning can also be a dominant mode of plasticity in Mg alloys. Experimental studies suggest that no single slip system or single twinning mode operates during the indentation of HCP single crystals such as Ti and Mg [9,10]. As a consequence, the simulations for Mg alloys in Refs. [22–25] were performed with multiple slip systems and various CRSS ratios among the slip systems in order to properly fit the experimentally measured hardness values as a function of the indentation direction.

5 Pop-In in the *P–h* Curves as the Elastic–Plastic Transition

In contrast to the Berkovich indentation, where the indenter is geometrically self-similar, the use of spherical indentation can be used to probe the elastic–plastic transition since the effective indentation strain increases linearly with respect to the ratio of the contact radius to the indenter radius, a/R. For carefully polished single crystals, spherical indentation results in an elastic stage

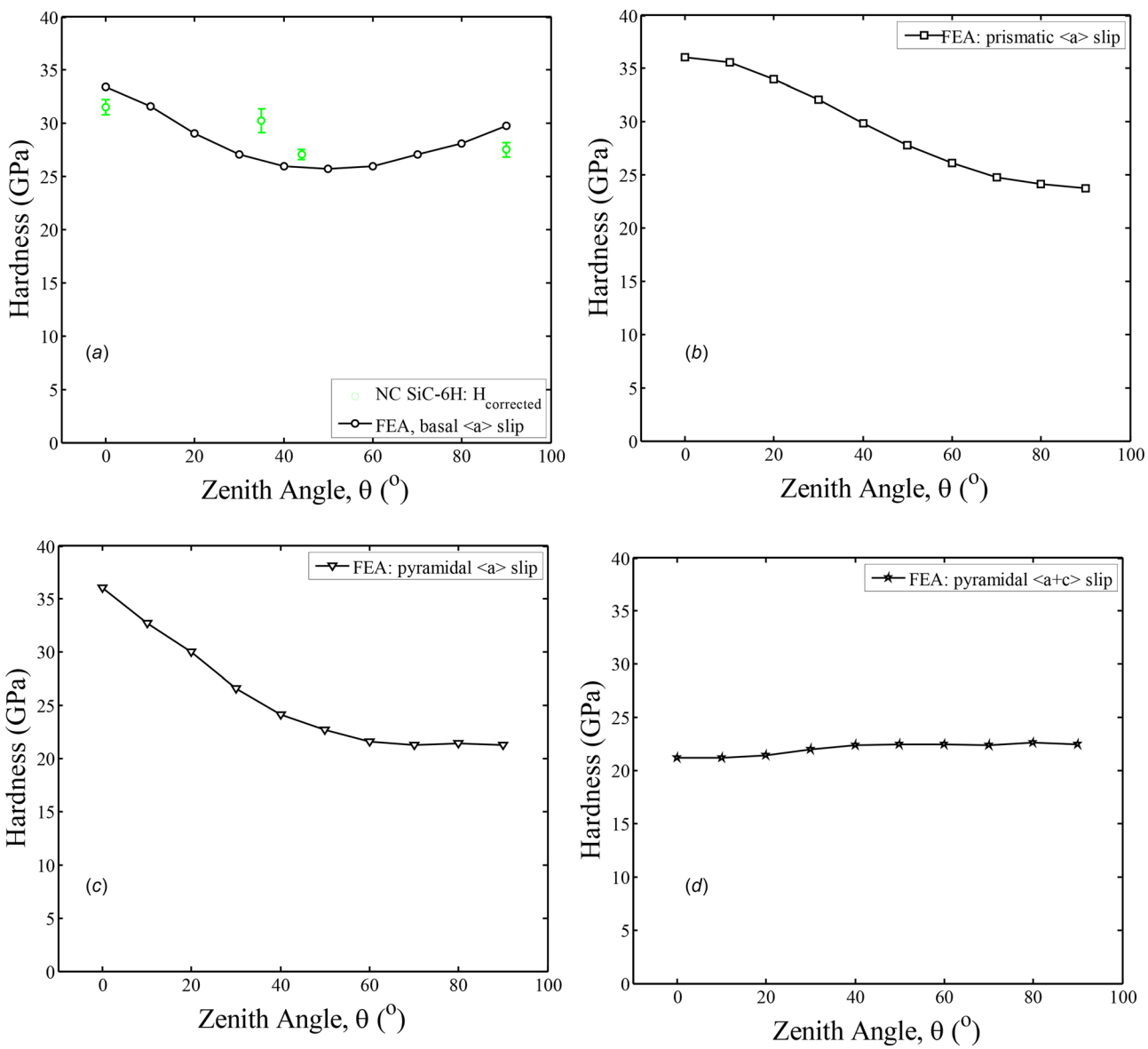

Fig. 3 A comparison of the experimentally measured hardnesses to those predicted from the crystal plasticity model assuming a CRSS, $\tau_{\text{CRSS}} = 4.8$ GPa, when only one type of slip is used: (*a*) basal, (*b*) prismatic, (*c*) pyramidal $\langle a \rangle$, and (*d*) pyramidal $\langle a + c \rangle$. The comparison suggests that the basal slip system dominates the deformation and thus the hardness anisotropy.

followed by a sudden displacement excursion in the load–displacement curve, denoted as "pop-in." The elastic response before pop-in in elastically isotropic materials can be described by Hertzian elastic contact theory. Previous pop-in studies for Mo and NiAl single crystals [16,28] suggest that for defect-free single crystals, the pop-in event corresponds to homogeneous dislocation nucleation in dislocation free regions, in which the maximum resolved shear stress inside the contact field reaches the theoretical strength of the material. The maximum resolved shear stress is given by

$$\max\left\{\tau_{\mathrm{RSS}}^{(\alpha)}\right\} = S_{\mathrm{ind}} p_0 = S_{\mathrm{ind}} \left(\frac{6PE_{\mathrm{r}}^2}{\pi^3 R^2}\right)^{1/3} \tag{3}$$

where p_0 is the maximum contact pressure, and the prefactor S_{ind} is defined here as the indentation Schmid factor since it is a measure of the ratio of the resolved shear stress to the applied stress, similar to the more traditional definition of the Schmid factor in uniaxial testing.

The pop-in loads measured for spherical indentation in Cree SiC-6H single crystals were converted to the pop-in shear stress based on Eq. (3) and the effective indentation modulus in Fig. 2. In Fig. 4, the pop-in stresses for spherical indenters with two different radii are observed to fall into the estimated bounds of the theoretical strength, that is, $G_{\{0001\}\langle 1\bar{2}10\rangle}/15 \sim G_{\{0001\}\langle 1\bar{2}10\rangle}/5$. The shear modulus on any shear plane and shear direction can be calculated from the Voigt elastic constants [29]; in this case, $G_{\{0001\}\langle 1\bar{2}10\rangle}$ is simply C_{44}. Umeno et al. [30]. have performed density functional theory (DFT) calculations and found a theoretical shear strength of 29.83 GPa for basal slip in SiC, which also falls into the hatched area in the figure.

The conversion from pop-in load to pop-in stress requires a knowledge of the indentation Schmid factor. Figure 5(*a*) shows that it varies in a parabolic manner with respect to the zenith angle. For the tests in Fig. 4, $S_{\mathrm{ind}} \approx 0.2$, as opposed to the commonly used factor of 0.31 that relates the maximum Mises stress to p_0 based on Hertzian contact theory with no consideration of discrete slip. Since the indentation direction may deviate from the assumed plane 1 shown in Fig. 1, we also include in Fig. 5 the results for plane 2 in Fig. 1. When pop-in occurs by homogeneous dislocation nucleation, we have $S_{\mathrm{ind}} p_0 = \tau_{\mathrm{th}}$. Using Eq. (3) gives

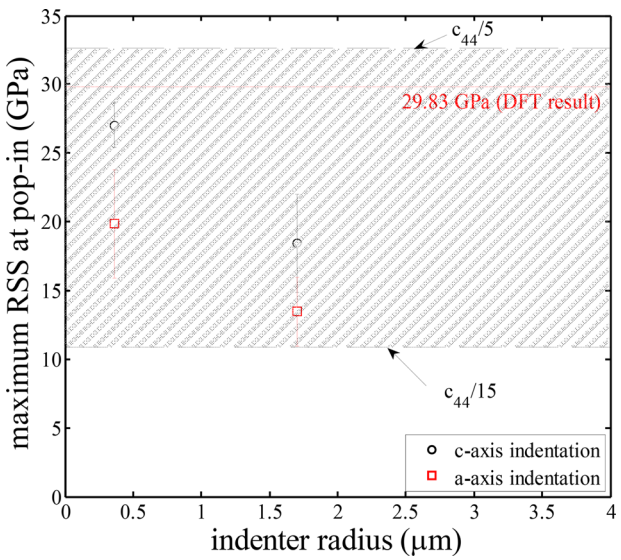

Fig. 4 Values of the maximum resolved shear stress on the basal slip system as a function of spherical indenter radius for Cree SiC-6H single crystals in two crystallographic orientations. The pop-in stresses are near the theoretical strength. No pop-ins were observed in tests using indenter with radii of 7.5 μm and 50 μm because the pop-in forces exceed the machine load capacity (500 mN).

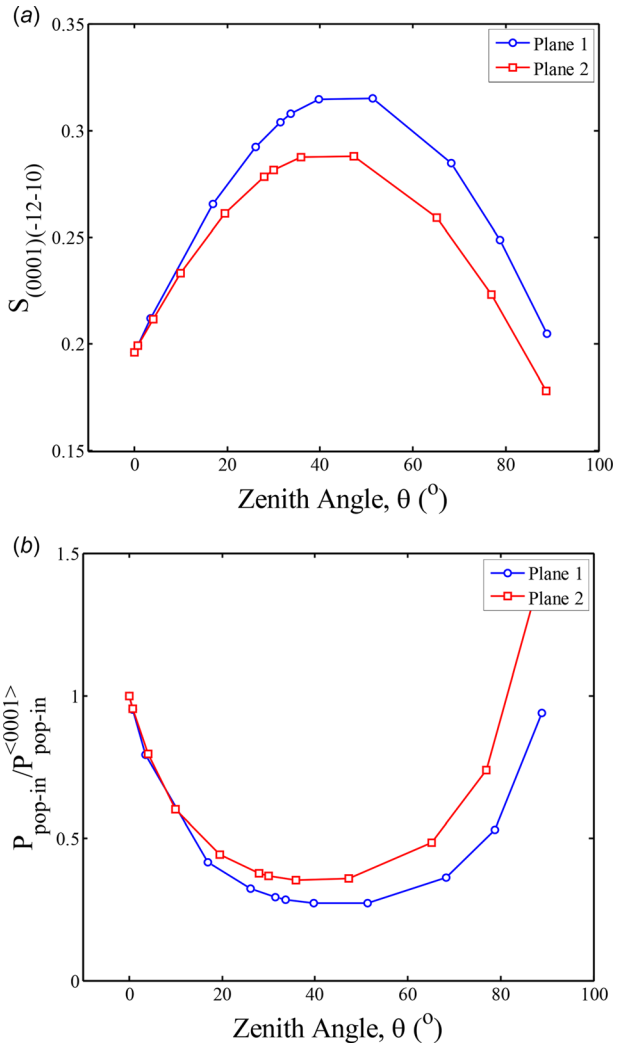

Fig. 5 (*a*) Indentation Schmid factor and (*b*) the predicted pop-in load as a function of the zenith angle in the two planes defined in Fig. 1(*a*) when only basal slip is allowed. Indentations in the *c* and *a* directions give almost the same indentation Schmid factor and pop-in load.

$$P_{\mathrm{pop-in}} = \frac{\pi^3 R^2}{6E_{\mathrm{r}}^2}\left(\frac{\tau_{\mathrm{th}}}{S_{\mathrm{ind}}}\right)^3 \tag{4}$$

whose dependence on the zenith angle is plotted in Fig. 5(*b*). Since the pop-in load is quadratic in the indenter radius, it becomes difficult to observe the homogeneous dislocation nucleation for larger indenter radii because there are limits to the loads that can be applied by the testing system ($\sim$500 mN for our experiments). In fact, for indenter radii of 7.5 and 50 μm, contact deformation in our experiments was entirely elastic with no pop-in observed up to the machine's maximum load capacity.

Several noteworthy findings are observed in Fig. 4. First, the pop-in stress indeed falls into the estimated bounds of the theoretical strength. One possible reason for the deviation from the DFT results is that there is a compressive normal stress component in the indentation experiments that is comparable to the resolved shear stress in the contact-induced stress fields, while the DFT calculations only consider pure shear without the normal stress. However, it is also notable that for large indenter radii, the stressed volume may be large enough to trigger heterogeneous dislocation nucleation if there are heterogeneous nucleation sites such as pre-existing dislocations in the vicinity of the contact [31,32]. This would produce a much lower resolved shear stress at

pop-in and may explain the decrease in pop-in stress with increasing indenter radius observed in Fig. 4. However, the dataset is too limited to draw a firm conclusion about this at this time.

6 Summary

This work demonstrates that the anisotropy in mechanical properties of single crystals can be quantitatively related to and examined from the anisotropy of the nanoindentation responses in different crystallographic directions. For SiC-6H single crystals, we have examined the indentation anisotropy of the effective contact modulus, hardness, and pop-in load. Salient observations include:

- After correcting the Oliver–Pharr method for pile-up effects, the measured and predicted values of the effective indentation moduli, $E_{\text{eff}}^{\text{SiC}-6\text{H}}$, agree well, despite the fact that the overall variation of $E_{\text{eff}}^{\text{SiC}-6\text{H}}$ against the zenith angle is only a few percent.
- The small degree of hardness anisotropy can be reproduced by crystal plasticity finite element simulations using just the basal slip system, as has been observed in the experiment [8]. Other slip systems give a totally different dependence of hardness on the zenith angle.
- The pop-in loads, when converted to the maximum resolved shear stress using the indentation Schmid factor, lead to pop-in stresses that agree with the theoretical strength for the basal slip system.

It is notable that even a weak anisotropy in the indentation response (changes in properties of only a few percent with changes in zenith angle) can be used to estimate the anisotropy in mechanical properties when aided by elastic and plastic contact analysis. In addition, even though the indentation responses of SiC-6H single crystals are generally close to isotropic (variations in properties of only a few percent in the elastic and plastic responses), one cannot treat the behavior as that of a Mises solid when examining polycrystalline SiC since there are only three slip systems (or two independent slip systems) available for the plastic deformation, which does not satisfy the Mises criterion for compatible deformation among neighboring grains. Thus, SiC polycrystals are generally quite brittle in the absence of strengthening grain boundary phases.

Acknowledgment

This research was supported by the U.S. National Science Foundation CMMI 0926798 (AD, LL, YFG) and DMR 1427812 (GMP), and the Natural Science Foundation of China 11425211 (YJW). Y.F.G. and G.M.P. are grateful to Dr. A.A. Wereszczak for his critical review of the manuscript.

References

[1] Pierson, H. O., 1996, *Handbook of Refractory Carbides & Nitrides*, Noyes Publications, Westwood, NJ.
[2] Snead, L. L., Nozawa, T., Katoh, Y., Byun, T. S., Kondo, S., and Petti, D. A., 2007, "Handbook of SiC Properties for Fuel Performance Modeling," J. Nucl. Mater., **371**(1–3), pp. 329–377.
[3] Yu, C. H., Bird, M. W., Huang, C. W., Chen, C. S., Gao, Y. F., White, K. W., and Hsueh, C. H., 2014, "Micromechanics Modeling of Creep Fracture of Zirconium Diboride-Silicon Carbide Composites at 1400–1700 °C," J. Eur. Ceram. Soc. **34**(16), pp. 4145–4155.
[4] Shaffer, P. T. B., 1964, "Effect of Crystal Orientation on Hardness of Silicon Carbide," J. Am. Ceram. Soc., **47**(9), p. 466.
[5] Niihara, K., 1979, "Slip Systems and Plastic Deformation of Silicon Carbide Single Crystals at High Temperatures," J. Less Common Met., **65**(1), pp. 155–166.
[6] Sawyer, G. R., Sargent, P. M., and Page, T. F., 1980, "Microhardness Anisotropy of Silicon Carbide," J. Mater. Sci., **15**(4), pp. 1001–1003.
[7] Page, T. F., Oliver, W. C., and McHargue, C. J., 1992, "The Deformation Behavior of Ceramic Crystals Subjected to Very Low Load (Nano)-Indentations," J. Mater. Res., **7**(02), pp. 450–473.
[8] Page, T. F., Riester, L., and Hainsworth, S. V., 1998, "The Plasticity Response of 6H-SiC and Related Isostructural Materials to Nanoindentation: Slip versus Densification," Mater. Res. Soc. Symp., **522**, pp. 113–118.
[9] Kwon, J., Brandes, M. C., Sudharshan Phani, P., Pilchak, A. P., Gao, Y. F., George, E. P., Pharr, G. M., and Mills, M. J., 2013, "Characterization of Deformation Anisotropies in an α-Ti Alloy by Nanoindentation and Electron Microscopy," Acta Mater., **61**(13), pp. 4743–4756.
[10] Catoor, D., Gao, Y. F., Geng, J., Prasad, M. J. N. V., Herbert, E. G., Kumar, K. S., Pharr, G. M., and George, E. P., 2013, "Incipient Plasticity and Deformation Mechanisms in Single-Crystal Mg During Spherical Nanoindentation," Acta Mater., **61**(8), pp. 2953–2965.
[11] Oliver, W. C., and Pharr, G. M., 2004, "Measurement of Hardness and Elastic Modulus by Instrumented Indentation: Advances in Understanding and Refinements to Methodology," J. Mater. Res., **19**(01), pp. 3–20.
[12] Shim, S., Jang, J.-I., and Pharr, G. M., 2008, "Extraction of Flow Properties of Single-Crystal Silicon Carbide by Nanoindentation and Finite-Element Simulation," Acta Mater., **56**(15), pp. 3824–3832.
[13] Vlassak, J. J., and Nix, W. D., 1993, "Indentation Modulus of Elastically Anisotropic Half-Spaces," Philos. Mag., **67**(5), pp. 1045–1056.
[14] Vlassak, J. J., and Nix, W. D., 1994, "Measuring the Elastic Properties of Anisotropic Materials by Means of Indentation Experiments," J. Mech. Phys. Solids, **42**(8), pp. 1223–1245.
[15] Gao, Y. F., and Pharr, G. M., 2007, "Multidimensional Contact Moduli of Elastically Anisotropic Solids," Scr. Mater., **57**(1), pp. 13–16.
[16] Li, T. L., Gao, Y. F., Bei, H., and George, E. P., 2011, "Indentation Schmid Factor and Orientation Dependence of Nanoindentation Pop-In Behavior of NiAl Single Crystals," J. Mech. Phys. Solids, **59**(6), pp. 1147–1162.
[17] Bolshakov, A., and Pharr, G. M., 1998, "Influences of Pile-Up on the Measurement of Mechanical Properties by Load and Depth Sensing Indentation Techniques," J. Mater. Res., **13**(04), pp. 1049–1058.
[18] Pharr, G. M., Herbert, E. G., Gao, Y. F., 2010, "The Indentation Size Effect: A Critical Examination of Experimental Observations and Mechanistic Interpretations," Annu. Rev. Mater. Res., **40**(1), pp. 271–292.
[19] Staroselsky, A. V., 1998, "Crystal Plasticity Due to Slip and Twinning," Ph.D. thesis, Massachusetts Institute of Technology, Cambridge, MA.
[20] Staroselsky, A., and Anand, L., 2003, "A Constitutive Model for hcp Materials Deforming by Slip and Twinning: Application to Magnesium Alloy AZ31B," Int. J. Plast., **19**(10), pp. 1843–1864.
[21] Gao, Y. F., Larson, B. C., Lee, J. H., Nicola, L., Tischler, J. Z., and Pharr, G. M., 2015, "Lattice Rotation Patterns and Strain Gradient Effects in Face-Centered-Cubic Single Crystals Under Spherical Indentation," ASME J. Appl. Mech., **82**(6), p. 061007.
[22] Sánchez-Martín, R., Pérez-Prado, M. T., Segurado, J., Bohlen, J., Gutiérrez-Urrutia, I., Llorca, J., and Molina-Aldareguia, J. M., 2014, "Measuring the Critical Resolved Shear Stresses in Mg Alloys by Instrumented Nanoindentation," Acta Mater., **71**, pp. 283–292.
[23] Kitahara, H., Mayama, T., Okumura, K., Tadano, Y., Tsushida, M., and Ando, S., 2014, "Anisotropic Deformation Induced by Spherical Indentation of Pure Mg Single Crystals," Acta Mater., **78**, pp. 290–300.
[24] Selvarajou, B., Shin, J. H., Ha, T. K., Choi, I. S., Joshi, S. P., and Han, H. N., 2014, "Orientation-Dependent Indentation Response of Magnesium Single Crystals: Modeling and Experiments," Acta Mater., **81**, pp. 358–376.
[25] Zambaldi, C., Zehnder, C., and Raabe, D., 2015, "Orientation Dependent Deformation by Slip and Twinning in Magnesium During Single Crystal Indentation," Acta Mater., **91**, pp. 267–288.
[26] Bower, A. F., Fleck, N. A., Needleman, A., and Ogbonna, N., 1993, "Indentation of a Power Law Creeping Solid," Proc. R. Soc. London A, **441**(1911), pp. 97–124.
[27] Su, C. J., LaManna, J. A., Gao, Y. F., Oliver, W. C., and Pharr, G. M., 2010, "Plastic Instability in Amorphous Selenium Near Its Glass Transition Temperature," J. Mater. Res., **26**(6), pp. 1015–1019.
[28] Bei, H., Gao, Y. F., Shim, S., George, E. P., and Pharr, G. M., 2008, "Strength Differences Arising From Homogeneous Versus Heterogeneous Dislocation Nucleation," Phys. Rev. B, **77**(6), p. 060103(R).
[29] Lee, J. H., Gao, Y. F., and Pharr, G. M., 2012, "Effective Poisson's Ratio From Combined Normal and Lateral Contacts of Single Crystals," J. Mater. Res., **27**(1), pp. 182–191.
[30] Umeno, Y., Kinoshita, Y., and Kitamura, T., 2008, "Ab Initio DFT Study of Ideal Shear Strength of Polytypes of Silicon Carbide," Strength Mater., **40**(1), pp. 2–6.
[31] Li, T. L., Bei, H., Morris, J. R., George, E. P., Gao, Y. F., 2012, "Scale Effects in the Convoluted Thermal/Spatial Statistics of Plasticity Initiation in Small Stressed Volumes During Nanoindentation," Mater. Sci. Technol., **28**(9–10), pp. 1055–1059.
[32] Bei, H., Xia, Y. Z., Barabash, R. I., Gao, Y. F., 2016, "A Tale of Two Mechanisms: Strain-Softening Versus Strain-Hardening in Single Crystals Under Small Stressed Volumes," Scr. Mater., **110**, pp. 48–52.